Journal of Materials Chemistry B

Accepted Manuscript

ROYAL SOCIETY OF CHEMISTRY

www.rsc.org/materialsB

Journal of Materials Chemistry B RSCPublishing

ARTICLE

Layered Double Hydroxide Nanoparticles to Enhance Organ-Specific Targeting and Anti-Proliferative Effect of Cisplatin

Cite this: DOI: 10.1039/xoxxoooooox

Received ooth January 2012,
Accepted ooth January 2012

DOI: 10.1039/xoxxoooooox

www.rsc.org/

Yue-Ming Kuo[a],‡ Yaswanth Kuthati[a],‡ Ranjith Kumar Kankala[a], Pei-Ru Wei[a], Ching-Feng Weng[a], Chen-Lun Liu[a], Ping-Jyun Sung[a,b], Chung-Yuan Mou[c] and Chia-Hung Lee[a]*.

To evaluate the role of charge in the nanoparticle distribution we modified the external surface of layered double hydroxide nanoparticles with various organic groups bearing different charges and further a near-infrared (NIR) fluorescent dye (Cy5.5) is conjugated in the layered structure to assess the biodistribution. The functionalized nanocomposites performed as highly efficient contrast agents since Cy5.5 molecule stabilization inside the layered structure can safe guard from metabolization in the physiological environments. The cell viability, lactate dehydrogenase and hemolytic assays showed no cytotoxicity with an exceptionally low release of both lactate dehydrogenase and hemoglobin from the treated cells. The *in vivo* biodistribution results disclosed a high accumulation of positive amino-Layered double hydroxides (LDHs) in the lung. In contrast, there is a rapid clearance of negatively charged carboxylate-LDHs from blood flow by liver uptake. Interestingly neutral LDH-PEG5000 showed enhanced blood circulation time, without high fluorescent accumulation in the major organs. In vitro cellular uptake studies from flow cytometry are relevant to the interactions between the nanoparticle surfaces and various cell types and the data are relevant to effects observed for *in vivo* biodistribution. To further demonstrate that surface functionalization on LDH nanoparticles can promote targeted drug release, we further immobilized hydroxo-substituted cisplatin (CP) on carboxylate-modified LDHs by the coordination bonding. Due to the ideal cleaving property of carboxylate group the coordinated CP can be efficiently released by increase of acidic proton and Cl^- concentration in the endosomal environment. Functionalized LDHs can be successfully employed as targeted drug delivery systems. When the LDH-CP complex accumulate primarily in the targeted organ, the high positive charge on the framework of LDHs cause susceptibility to rapid endocytosis, which facilitates sustained drug release with minimal systemic toxicity providing the apt treatment in the targeted organ.

Introduction

In the recent years significant progress has been made in nanomedicine by fusing inorganic nanomaterials with biology and biochemistry to deliver drugs and imaging agents to the target sites. Layered double hydroxides (LDHs), a class of hydrotalcite-like compounds, are gaining increasing attention as a carrier in drug delivery.[1-21]

[a]Department of Life Science and Institute of Biotechnology, National Dong Hwa University, Hualien, 974, Taiwan. [b]Graduate Institute of Marine Biotechnology, National Dong Hwa University, Pingtung 944, Taiwan. [c]Department of Chemistry, National Taiwan University, Taipei, 106, Taiwan. ‡These authors contributed equally.*corresponding author, E-mail: chlee016@mail.ndhu.edu.tw Electronic Supplementary Information (ESI) available: TEM images, UV-Vis spectra and white-light sample images, microscopic morphological examination, MTT cytotoxicity assay, Lactate dehydrogenase assay, DNA fragmentation. See DOI: 10.1039/b000000x

LDHs possess lamellar structure with positive layers containing bivalent (Mg(II) in our case) and trivalent metal ions (Al(III)). The positive charges of the layers are balanced by intercalation of anions, which can be exchanged with other large anions. With the unique ion-layer charge interaction in the super-molecular structure, many theranostic agents could be intercalated within the LDH structure via ion-exchange to form smart LDH nanohybrids which could then function as a slow-release carrier. LDHs have been shown to be a carrier for negatively charged species of biomedical functions, such as DNA,[22-28] siRNA,[29] antibodies,[30] carbohydrates,[31] enzymes,[32] negatively charged antimicrobial drugs,[33, 34] anti-inflammatory drugs[35] and anticancer drugs[14,36] or other bioactive molecules.[37-44]

As a nanocarrier, LDH shows many advantages over other inorganic carriers. First, they tend to exhibit low cytotoxicity,[45-48] even at high dose. In addition, the LDH is easily degraded in

acidic environment thus endowing it a biodegradable advantage. The net positive charge on LDH facilitates its easy cell-uptake by interacting with the negatively charged biological membranes. LDH nanoparticles are shown to mitigate the effects of drug resistance by releasing the cargo in the cancer cells through a unique clathrin-mediiated endocytosis mechanism[49] and further they are shown to enhance the cellular recognition when modified with cell targeting ligands like folic acid.[50] Also, LDH had been shown to exhibit favorable blood clearance profiles compared to free drug, prolonging drug half-life in blood stream, and thus better targeting ability towards targeting site.[51, 52] The interlamellar structure of LDH materials have facilitated the integration of not only multiple types of drug[53-56] but also drugs in combination with imaging agents[57-59] in one system for combinational chemotherapy to eradicate drug resistance and for the simultaneous evaluation of bio distribution and bio imaging. LDH materials have also been fabricated with other nanoparticles as this design can exploit the advantages of two or more nanoparticles in a single nano construct with multiple functions. On one hand the fabrication of LDH material with other nanoparticles has shown to increase the stability[60, 61] and dispersity[62] of nanoparticles. On the other hand it has shown to impart beneficial properties such as targeting ability,[63] controlled drug release,[64-70] easy particle functionalization,[68] improved biocompatibility[71-73] and enhanced photostability and contrast efficacy of imaging agents.[57, 74-77]

Although LDH possesses the many good features as a nanocarrier in biomedicine as listed above, the materials aspects still need a lot of developments before it can fulfill its rich potential in nanomedicine. For better control of the LDHs' movement through various biological barriers in an in vivo study, one needs good control in the size, morphology and surface character of the nanomaterials. Unlike the much well-developed materials such as silica, synthetic controls of LDH are less developed. Recently, better size control of the nanoparticles of LDH has been reported through judicious choice of surface protecting agents in synthesis[78-80] On the other hand surface functionalizations of LDH in the context of drug carrying/releasing and its biodistribution have been less studied.[81] These are important especially when one is trying to deliver highly toxic drugs to specific organs or sites. In one recent study Zhu and colleague's reported the delivery of cisplatin prodrug using non-functionalized LDH materials. It was reported that LDH loaded produg was highly cytotoxic to cancer cells than the free drug. Further it was demonstrated that pro drug intercalated LDHs were less cytotoxic against certain kinds of normal cells.[82]

One needs a good strategy for directing the biodistribution of LDH nanoparticles in an *in vivo* studies. Also for loading various kind of drugs, one need rich repertoire of surface functionalizations. In our previous communication we have reported chitosan coated LDH-Indocyanine green nanoparticles for efficient in vivo optical imaging.[74] In this communication we report that proper surface functionalizations of LDH can help in loading neutral molecule and further direct the nanoparticles to specific organ.

We choose to study the loading of cisplastin (CP) into LDH with a specific design of the surface functionalization of CP to help the loading and release. Clinical use of CP has been constrained by several factors, e.g. poor solubility, bad circulation, high toxicity and nerve damage.[83, 84] In view of the above, this article reports the conjugation of CP molecules to the carboxylate-modified LDH surfaces (Fig. 1e). Carboxylate modifications possess the ideal property that facilitates cisplatin release in the form of CP-carboxylate complexes under the endosomal acidic pH value and replacement by Cl^- (or H_2O) in the cytosol. This unique strategy of functionalizing LDH with a carboxylate group can significantly increase the therapeutic efficiency by maintaining high concentrations of drug at the disease foci. Hence the drug dosage can be significantly reduced thereby minimizing the systemic toxicity. We have also examined the cytotoxicity of LDH nanoparticles by conducting in vitro toxic assays. Finally, we study the effect of surface functionalities on the biodistribution of LDHs. For this purpose, four different LDHs (Cy5.5-functionalized) with different functional groups will be synthesized, e.g. (a) amine-functionalized LDH-NH_2, (b) PEGylated LDH-NH-PEG5000, and (d) carboxylated LDH-NH-COOH samples. We will use the fluorescence tag to measure the biodistribution of the LDHs in dissected organs from a mouse sacrificed after i.v. injection of the LDHs. We will show surface functionalization will affect strongly the fate of the LDHs in mouse after injection.

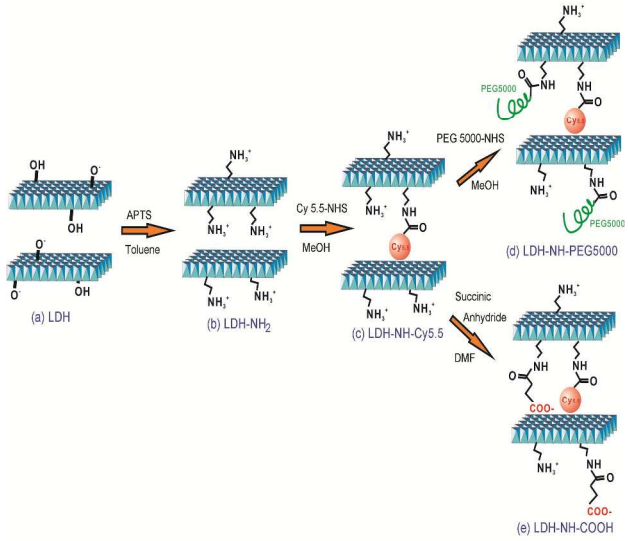

Fig. 1 Schematic representation (a) LDH nanoparticles, (b) the modification of amino groups on LDH surfaces by reaction with APTS, (c) the conjugation of Cy5.5 in the surfaces of LDH-NH_2 samples, (d) the further conjugation of LDH-NH-Cy5.5 with PEG-5000, and (e) the further modification of LDH-NH-Cy5.5 surfaces with carboxylate groups by reaction with succinic anhydride.

The use of LDH as an organ-specific targeting agent has the benefit of regulating the nanoparticle distribution in specific

organs by attaching different charged functional groups using the surface modification as shown in Fig. 1.

Experimental

Materials

$Mg(NO_3)_2.6H_2O$, $Al(NO_3)_3.9H_2O$, PBS (dry powder), and 3-(4,5-dimethylthiazol-2-yl)-2,5-diphenyltetrazolium bromide (MTT), succinic anhydride, Methoxypolyethylene glycol 5000 acetic acid N-succinimidyl ester were purchased from Sigma-Aldrich (St Louis, USA). 3-Aminopropyl- trimethoxysilane (APTS), Trichloroacetic acid (TCA), NaOH, toluene and DMF were purchased from Acros (Geel, Belgium). Potassium bromide (KBr-FTIR grade) was purchased from Fisher Scientific Ltd (Leicestershire, UK). Ninhydrin was purchased from Alfa Aesar (Ward Hill, Massachusetts, UK). RPMI-1640 medium, fetal bovine serum, penicillin, and streptomycin were obtained from GIBCO/BRL Life Technologies (Grand Island, NY, USA). Cy5.5 NHS ester purchased from GE healthcare UK ltd (Buckinghamshire UK). RBCs and blood plasma (goat) are a gift from Hualien District Agricultural Research and Extension Station, Taiwan.

Instruments

Centrifugation during nanomaterials synthesis was performed at an appropriate temperature using Hermle Z 36 HK (Wehingen, Germany) instruments, respectively. UV-vis absorbance was recorded on Genequant-1300 series spectrophotometer and fluorescence imaging was captured using Typhoon-FLA 9000 bimolecular imaging system (Imagequant TC-7.0). MTT absorbance was recorded using Perkin Elmer's EnSpire Multi-label Plate Reader (Santa Clara California, USA).

Characterization

FT-IR spectra were recorded on a Bruker Alpha spectrometer with a dried KBr pellet. The particle size and ζ-potentials of various LDH samples were measured in a Malvern Nano-HT Zetasizer. The ζ-potential distribution was obtained by an average of ten measurements.

Synthesis of LDH nanoparticles. The LDH nanoparticles for this report were prepared using a co-precipitation method which was given previously.[85-88] To prevent the contamination by atmospheric CO_2, dd-H_2O was decarbonated by boiling before it was used in all of the preparations. Briefly, 0.769g of $Mg(NO_3)_2 \cdot 6H_2O$ and 0.357g of $Al(NO_3)_3 \cdot 9H_2O$ were dissolved in 10 mL dd-H_2O followed by the quick addition of 40 mL NaOH solution (0.15 M) by stirring under room temperature for 10 min. Finally, the nanoparticles were washed with 40 mL of dd-H_2O and centrifuged at 25,000 rcf for 10 min. The as-synthesized products were recovered and further suspended in 50 mL dd-H_2O, and the solution was hydrothermally treated at 100 °C for 16 h. Finally, the resulting LDH were recollected by centrifugation (25,000 rcf, 10 min), washed repetitively with ethanol and stored for further usage.

Synthesis of LDH-NH_2. To improve the binding affinity between APTS-LDH complexes toluene used as the reaction solvent because the condensation of APTS molecules on LDH surfaces can be carried out efficiently at a high reflux temperature. The general reaction conditions as follows: 0.2 g of the as-synthesized LDHs were placed in 30 mL toluene and stirred for 30 min followed by the addition of 1.0 mL APTS. The reaction is carried out at 100 °C for 24 h, followed by withdrawing via centrifugation (25,000 rcf, 10 min, at 4 °C), and washed thoroughly with acetone and ethanol. The nanoparticles are dispersed in ethanol for further modification.

Synthesis of Cy5.5-labeled LDH-NH_2. Cy5.5-conjugated LDH-NH_2 complexes were synthesized by stirring 1 mg of Cy5.5 NHS ester with 40 mg of LDH-NH_2 in 0.5 mL of dry methanol in the dark for 12 h. The particles were recovered by centrifugation (25,000 rcf, 10 min, at 4 °C), and thoroughly washed twice with ethanol.

Synthesis of LDH-NH-COOH. The modification of carboxylate groups in LDH-NH_2 and Cy5.5-labeled LDH-NH_2 surfaces is carried out in the following way: 10 mg of LDHs-NH_2 (or Cy5.5-labeled LDH- NH_2) samples are suspended in 6.0 mL of anhydrous DMF and were further reacted with 40 mg of succinic anhydride at room temperature under continuous stirring for 24 h. The particles were recovered by centrifugation (25,000 rcf, 10 min) and thoroughly washed with ethanol.

Synthesis of LDH-NH-PEG5000.

10 mg of LDHs- NH_2 (or Cy5.5-labeled LDH-NH_2) samples were suspended in 3.0 mL of anhydrous methanol, and further reacted with 6 mg of PEG5000-NHS at room temperature under constant stirring for 24 h. The particles were collected by centrifugation (25,000 rcf, 10 min) and thoroughly washed with ethanol.

Coordination of CP onto the LDH-COOH samples. To increase the reactive concentration of CP in aqueous solution, the chloro ligand of the CP molecules was replaced by the hydroxo ligand through the reaction of CP (20 mg) in $AgNO_3$ solution (23 mg in 1.5 mL dd-H_2O). The reaction was carried out for 12 h at 37 °C in dark. After the reaction, a white precipitate of AgCl is removed by centrifugation (25,000 rcf, 20 min). The supernatant containing highly water soluble CP is adjusted to a pH value of 6.8 and diluted to 4 mL by adding dd-H_2O. The LDH-COOH-CP complexes were synthesized by the addition of LDH-NH-COOH samples (10 mg) in 4 mL of CP solution the mixtures were shook under 37 °C and stored in dark conditions for 12 h. The LDH-COOH-CP solids and the un-coordinated free hydroxo-CP particles were separated by centrifugation (25,000 rcf, 20 min, at 4 °C) and further washed several times and redispersed in dd-H_2O. The surface concentration of cisplatin conjugated particles is determined by measuring the change in absorbance at 276 nm. Calibration experiments were conducted separately before each set of measurements with cisplatin of different concentrations.

***In vitro* drug release study.** In a typical drug release study, 5 mg of hydroxo-substituted cisplatin coordinated LDH-NH-COOH samples were suspended in 1 mL of buffer mimicking with endosome pH-5.0 and physiological saline pH-7.4 (0.1 M phosphate buffered saline) and maintained in 37 °C at 300 rcf to mimic the pathophysiological

conditions. Aliquots were removed at regular intervals by centrifuging at 25,000 rcf for 10 min and supernatant was analyzed by UV at λ_{max} 360 nm and it was continued by replacing the respective fresh simulated fluids at their respective time points. The release amount in the solution phase was determined by UV-Vis spectrophotometer and the cumulative % drug release was calculated.

Cell culture

Sulforhodamine B assay. 1×10^4 HT-29 cancer cells were seeded onto 96 well plates containing RPMI-1640 medium with 10% fetal bovine serum and incubated in 5% CO_2 at 37 °C overnight. After adhering, one group of the cell line was fixed *in situ* with 25 µL of 50% (w/v) trichloroacetic acid (TCA) to determine the cell number at the time the cells received the tested drug (T_0). For the other groups, various drug concentrations in serum free medium were added and incubated for 4 h and the same volume of 20% FBS medium was added for treatment up to 20 h (T_x groups). After 24 h of drug treatment 50 µL of cold TCA was added to the T_x groups and the control group (Ctl: no drug treated wells) and incubated at 4 °C for 1 h. Further, the medium was removed by suction, and washed three times with dd-H_2O (200 µL in each well) and air dried for 12 h. Then, 100 µL of 0.4 % (w/v) sulforhodamine B solution prepared in 1 % acetic acid were added to each well, and the plates were incubated for 20 min at room temperature. The unbound sulforhodamine B was removed by washing three times with 1 % (v/v) acetic acid. The bound sulforhodamine B was subsequently dissolved by adding 10 mM of trizma base (pH 10.5) eventually the absorbance was measured at 515 nm. The percentage of growth inhibition is defined as $100-[(T_x-T_0)/(Ctl-T_0)]\times100$ (when $T_x\geq T_0$). GI50 (concentration of 50 % cell growth inhibition) is defined as $(100-[(Tx-T0)/(Ctl-T0)]\times100)= 50$ and calculated by the Sigma Plot software.

DNA fragmentation assay. HT-29 cells (1×10^6/mL) were treated with or without drug for 24 h, washed with PBS twice, lysed in cell lysis solution, and then pipetted until no visible cell clumps remained. Genomic DNA was purified by the Wizard Genomic DNA purification kit (Promega, Madison, Wisconsin, USA). After isopropanol precipitation, samples of 10 µg were loaded in each lane. The pattern of DNA cleavage was analyzed by 2.0% agarose gel electrophoresis at 100 V for 1.5 h in Tris-borate/EDTA electrophoresis buffer.

Hemolysis assay. The method for hemolysis assay has been reported previously.[74] Heparin-stabilized goat blood samples were freshly obtained from the Hualien District Agricultural Research and Extension Station, Taiwan. A mixed sample of 5 mL blood and 10 mL PBS was centrifuged at 25,000 rcf for 10 min, the pellet of RBCs was washed with PBS (10 mL) five times, and then 50 mL of PBS was added for further dilution. To evaluate the hemolysis of the various concentrations of nanoparticle exposure, the leach of red hemoglobin in the supernatant was correlated by visual observation of color with the positive and negative control experiments by incubation of RBCs with dd-H_2O and PBS, respectively. The treated condition was as the following. A 200 µL of diluted RBC suspension was added to 800 µL of different concentrations of LDH in PBS solution by vortex and then the mixture samples were kept at room temperature for 3 h.

Comet assay. The DNA breakage is evaluated using a comet assay kit (Trevigen, Gaithersburg, MD, USA) by following the manufacturer's instructions. Immediately prior to imaging, comet slides with DNA smear were hydrated and stained with SYBR green (Trevigen) for 15 min. Comets were analyzed using a fluorescence digital imaging system**.**

LDH release assay. HT-29 human colon cancer cells were seeded on 12-well plates (1×10^5 cells/ml). The cells were grown in 10% FBS- supplemented RPMI-1640. The level of cytosolic LDH (lactate dehydrogenase) leakage was assessed to measure the extent of cellular membrane damage by using Sigma Tox-7 Kit (Sigma-Aldrich, St Louis, USA) following manufacturer's instructions. This kit determines the LDH activity spectrophotometrically by measuring the intensity of red color formed by the reduction of formazan at 490nm, which is directly proportional to the LDH activity. The optical absorbance was measured by ELISA reader. Results given represent mean values from triplicate measurements. Results are given as fractional LDH release compared to the positive control consisting of 1% Triton X-100 (yielding 100% LDH release). The LDH content of each sample was calculated according to the following formula: Cytotoxicity (%) = [(experimental value−low control)/ (high control−low control)] × 100.

Cell uptake. For determination of uptake of modified LDHs by different cells, $1x10^6$ of cells were plated in 10 cm dishes and incubated for 24 h at 37 °C and 5% CO_2. After adhering, cells were then exposed to 50 µg mL^{-1} of various LDH samples in 10% FBS serum medium and incubated for 1 h at 37 °C. All treated cells were then washed twice with PBS, trypsinized and analyzed by flow cytometry (BD Accuri C5). For fluorescent microscopic imaging, HT-29 cells were treated with Cy 5.5-LDHs (50 µg mL^{-1}) for 4 h at 37 °C in serum-free medium followed by phosphate buffered saline (PBS) wash and fixingwith 4% paraformaldehyde at room temperature for 10 min. The cells were washed with PBS three times and incubated with 0.2% Triton X-100 and then 3% bovine serum albumin in PBS for 5 and 30 min, respectively. Rhodamine phalloidin was used for staining the filamentous actin skeleton at room temperature for 20 min. The nucleus was stained with 4',6-diamidino-2-phenylindole (2 µg mL^{-1}) in H_2O for 5 min. Cells were visualized under a fluorescence microscope.

Biodistribution studies. All experiments involving animals were reviewed and approved by the Administrative Committee of Animal Experiments, Department of Life Science and the Institute of Biotechnology, National Dong Hwa University. All procedures were performed in accordance with the guidelines of the Management Group of Animal Experiments in Taiwan. The male nude mice (20 g, 6–8 weeks old) were purchased from BioLasco Taiwan Co., Ltd and housed in a light (12 h)/dark (12 h) cycle with food and water. For *in vivo* biodistribution experiments, sixteen mice were divided into four groups and thus each group had four mice. We studied the *in vivo* biodistribution experiments of the control (only treated with physiological

saline), LDH–NH_2, LDH–NH–PEG5000, and LDH–NH–COOH groups. Before the imaging experiments, the mice were not fed for 12 h to minimize rodent chow autofluorescence within the GI-tract, and they were anesthetized by urethane (1.5 g kg^{-1}) i.p. injection. Mice received an i.v. tail vein injection of approximately 50 uL of LDH samples at the dosage of 5 mg kg^{-1}. This dosage is well tolerated by the mice and no side effects were observed during the experimental period. Finally, the animals were sacrificed by a CO_2 overdose. Major organs were then harvested intact, and imaged for fluorescence using a fluorescent imaging system. Fluorescent imaging was carried out on a Typhoon FLA 9000 Biomolecular imager. The light was passed through fluorophoredependent bandpass interference filters to induce Cy 5.5 fluorescence. The imaging detector was a 250 V of PMT. Bandpass interference filters were used to pass fluorescence, but block excitation light.

Results and discussion

Fig. 1 represents the modification of LDH surface with various organic groups. Initially, the amino groups are immobilized on the surface of LDH by the co-condensation of APTS molecules at a high temperature (Fig. 1b). The resulting amino-LDH surface can be utilized as an active site for further coupling reaction. Cy5.5 fluorescent dye was conjugated to the amine group through a simple coupling reaction (Fig. 1c). As shown in Fig. 1(d) and (e) the residual amino groups were conjugated to PEG5000-NHS and succinic anhydride to form LDH-NH-PEG5000 and LDH-NH-COOH complexes, respectively.

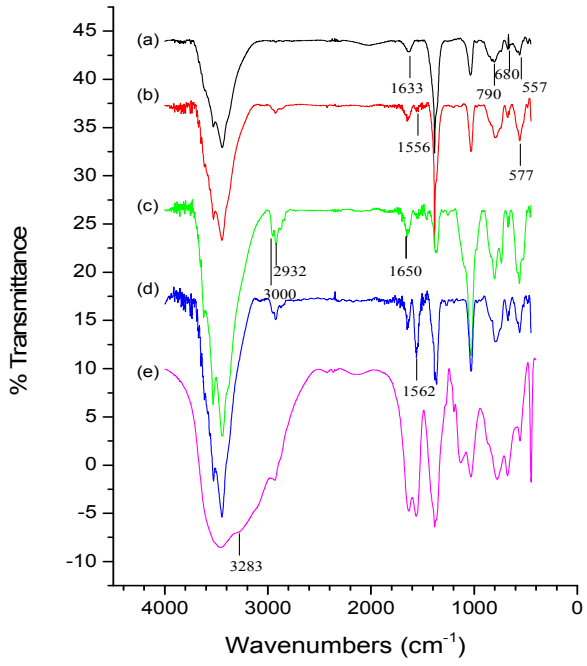

Fig. 2 FT-IR spectra of (a) LDH, (b) LDH-NH_2, (c) LDH-NH-PEG5000, (d) LDH-NH-COOH and (e) LDH-NH-COOH-CP samples.

Fig. S1 (See Supporting Information) represents the TEM imaging of LDH samples functionalized with different terminal groups. The LDH-NH_2 and LDH-NH-COOH samples showed a hexagonal shape and uniform size with an average particle diameter of 150-200 nm. However, the TEM images of the PEG5000-modified LDH samples (Fig. S1c) showed a round shape surrounded by the elastic scattering of electrons which confirms the binding of PEG layer selectively to the LDH surface. To investigate the stability of LDH-NH-COOH-CP we soaked the particles in a blood plasma for 24 h. We observed no degradation of LDH frameworks (Fig. S1d). We can infer that the release of CP from the LDH-NH-COOH-CP sample may arise from the pH-sensitive mechanism that can contribute to the drug release under acidic pH of endosomes. We employed FT-IR spectroscopy to characterize the chemical bonds and surface organic groups in LDH samples (Fig. 2). The spectra of bare LDHs showed a broad band (3100-3700 cm^{-1}) from the O-H stretch of the absorbed molecular H_2O. The band at 1633 cm^{-1} is presumably caused by H_2O deformation. The bands at 790, 680, and 557 cm^{-1} are attributed due to the vibration of (M–O) and (M–O–M) (M= Mg or Al). These bands were also observed in all functionalized LDH samples. In the amino-functionalized LDH sample (Fig. 2b), the presence of APTS(–$Si(CH_2)_3$ NH_2) functional group on the wall surface is confirmed by the presence of the N–H (primary amine) bending vibration at 1556 cm^{-1}, and C–H stretching at 2932 cm^{-1}. After APTS modification, the M–O vibration at 577 cm^{-1} showed higher intensity than the bare LDH samples because of the overlapping of Si–O–Al vibrations (577 cm^{-1}) with the APTS grafted LDH samples. Either PEG-5000 or carboxylate groups were conjugated to the amino-modified LDHs through a simple coupling reaction. The PEG-5000 molecule has an activate N-hydroxysuccinimide (NHS) group, which is an amino-reactive chemical bond (NHS-ester) to facilitate the coating of PEG-5000 on LDH surfaces. It exhibited an increase in the intensity of C–H stretch at 2932 cm^{-1} because of PEG-5000 backbone contribution and the weaker band at 3000 cm^{-1} may arise from the Fermi resonance overtone of the N-H stretching band of secondary amides. In addition, the production of a C=O stretch mode from the terminal group of PEG-5000 was also observed which confirms overlap with the H_2O deformation at approximately 1650 cm^{-1} (Fig. 2(c)). Another band from the N-H bend of the secondary amide is observed around 1562 cm^{-1}. After conjugating carboxylate groups on amino-LDH surfaces, it is observed that the peak intensity of N-H bend at 1562 cm^{-1} is higher than the LDH-NH-PEG 5000 sample; however, the peak intensity of C–H stretch at 2932 cm^{-1} was relatively low. We can refer the variation in the two peak intensities of the carboxylate modified LDH sample to the reaction of the amino-LDH surfaces with succinic anhydride. When the amino groups were reacted with succinic anhydride, a complete reaction was achieved (see Fig. 2(d)).

Therefore, the LDH-NH-COOH surfaces can yield more N-H groups (from secondary amide) than the LDH-NH-PEG 5000 sample and thus the LDH-NH-COOH sample showed much contribution to the vibration intensity at 1562 cm^{-1}.

However, the succinic anhydride molecule has shorter backbone than the PEG-5000 molecules; therefore the LDH-NH-COOH sample provides less C-H vibration than the PEG-5000-modified LDHs. We can observe a relatively low intensity of C-H vibration at 2932 cm^{-1} in the LDH-NH-COOH sample. After further conjugation of hydroxy substituted cisplatin to the carboxyl end of the LDH-NH-COOH sample, an increase of intensity around 1640-1560 cm^{-1} was contributed from the different N-H bending modes of coordinated cisplatin molecules in LDH-NH-COOH surfaces. In addition, a very broad peak around 3400-2400 cm^{-1} is attributed to O-H stretch of hydroxo-cisplatin molecules and overlaps the C-H and N-H stretch in this ranges (Fig. 2(e)).

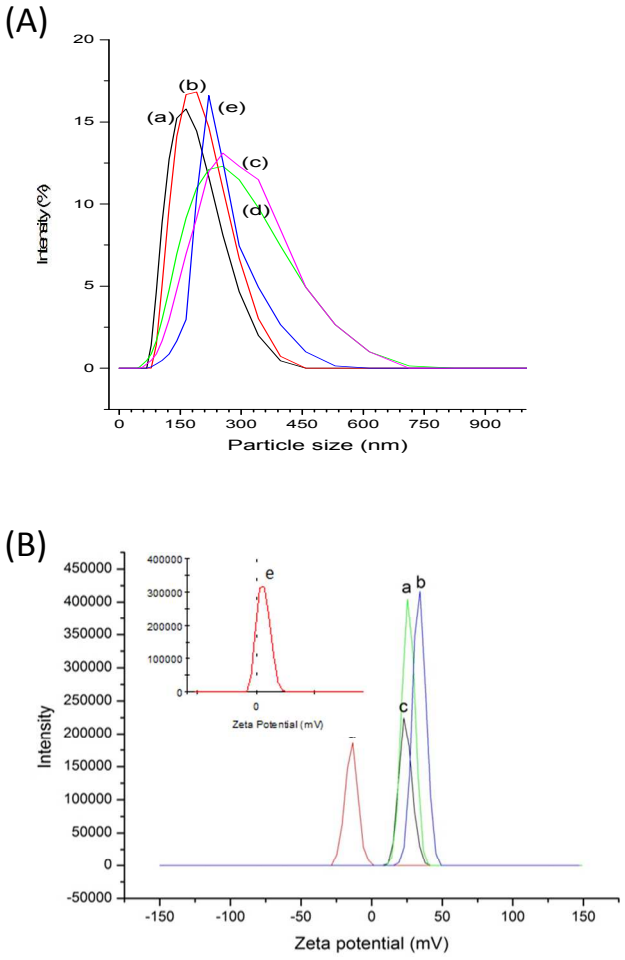

Fig. 3 (A) Particle size and (B) Zeta-potential distribution at pH 7.4 of (a) LDH (156 nm, +26 mV), (b) LDH-NH_2 (221 nm, +35 mV), (c) LDH-NH-PEG5000 (268 nm, +22 mV), and (d) LDH-NH-COOH (246 nm, -13 mV) (e) LDH-NH-COOH-CP (252 nm, +5.94) inset figure.

To verify the existence of different charges on the surface functionalized LDH samples, we measured the ζ-potential of LDH samples in aqueous solution at pH 7.4 (Fig. 3 B). Results showed a more positive ζ-potential on LDH surfaces, which can be attributed to the presence of metal (Al^{3+} and Mg^{2+}) hydroxides of +26 mV (Fig. 3 B(a)). The surface modification with positively charged amino groups exhibited a significant increase in the ζ-potential to +35 mV (Fig. 3 B(b)). The further conjugation of PEG5000 molecules on the LDH-NH_2 sample decreased the ζ-potential to +22 mV (Fig. 3 B(c)) which arises from the reaction of amino groups in LDH surfaces with neutral PEG5000 molecules. For the conjugation of carboxylic groups with amine modified LDH's, succinic anhydride was chosen to react with amino groups of LDH-NH_2 through a ring opening reaction. The modification of negative charges of carboxylate groups in LDH-NH_2 surfaces showed a further decrease of ζ-potential from +35 mV of LDH-NH_2 to -13 mV in LDH-NH-COOH samples (Fig. 3 B(d)) and eventually after coordination with cisplatin the potential had a shift towards positive side with +5.94 mV denoted in inset figure of Zeta potential (Fig. 3 B(e)). It is clear from the graphical representation of DLS measurements related to size that all the samples are in accord with in the size range of 150-250 nm (Fig. 3A) which was the most suitable array in blood circulation. Compared with the TEM images, the DLS results of LDH samples showed a larger particle size distribution. We can refer the large size distribution of DLS from the hydrodynamic diameters of organic ligands in LDH surfaces. The changes in the ζ-potential of various modifications of LDH samples provided additional evidence besides FT-IR to demonstrate that different functional groups were attached to the surface of LDHs.

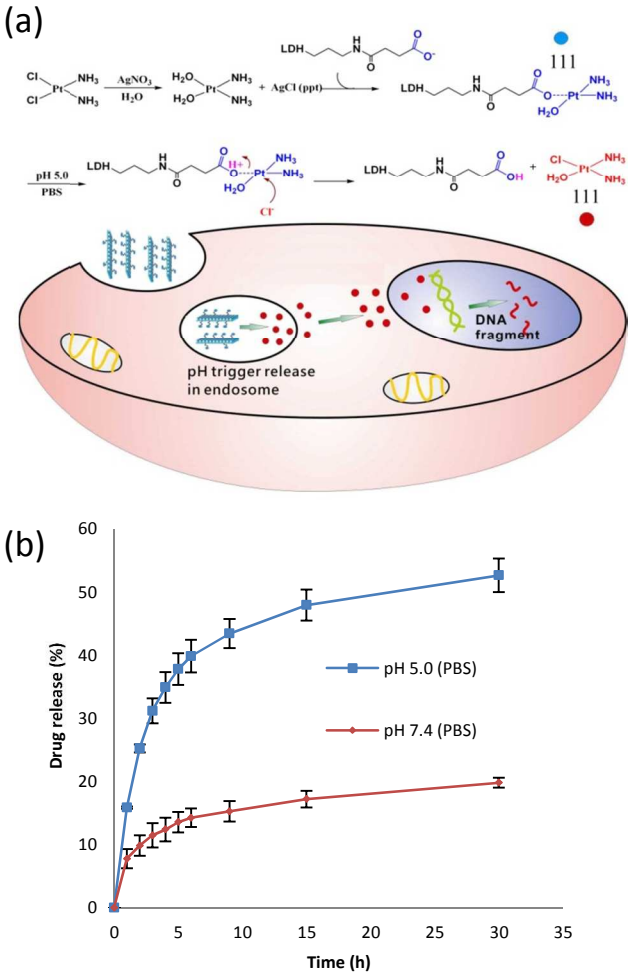

Fig. 4 (a) Schematic representation of intracellular release of cisplatin into colon cancer cells by immobilization of hydroxo-substituted cisplatin on carboxylate-modified LDHs. Release of cisplatin can be achieved by the replaced effect from the acidic pH and Cl^- in endosomes. (b) Release curve of hydroxo-substituted cisplatin in various pH namely 5.0 (endosome pH) and 7.4 (PBS).

Fig. S2 showed UV-Vis spectra and photographic sample images of samples after various surface functionalizations of LDHs. Ninhydrin tests were run to quantify the primary amines at the surface of modified LDH samples using the following procedure. For the analytic process, we treated the LDH samples with ninhydrin for 30 min in an ethanol solution and that react only with primary amines of LDH-NH_2 to produce Ruhemann's purple, which display characteristic absorption band at 580 nm, however, ninhydrin cannot react with secondary amines. After the reaction, we centrifuged out the solid nanoparticles, and the UV-Vis spectrum of the solution phase showed a characteristic absorption of Ruhemann's purple at 580 nm (Fig. S2(a)). In addition, the production of Ruhemann's purple was also observable in the sample color. This phenomenon indicated that large amounts of amino groups were modified in the LDH-NH_2 samples. If we compare the absorbent intensity of Ruhemann's purple between LDH-NH-PEG5000 (Fig. S2(b)), and LDH-NH-COOH (Fig. S2(c)) samples, the LDH-NH-COOH sample has lower intensity. This phenomenon indicates that most amino groups in the LDH-NH-COOH sample have completely reacted with succinic anhydride; thereby, efficiently immobilizing the CP molecules through the coordination of carboxylate groups with platinum. The reactivity of ninhydrin with various functionalized LDH samples can provide us an additional evidence to confirm the chemical modifications on the LDH surfaces. Fig. S3 showed the UV-Vis spectrum of the hydroxo-cisplatin sample. An absorbance at about 250 nm is attributed to the d-d band of Pt(II), which is hidden by the electron-transfer band (peak maximum 210 nm). For the spectrum of the LDH-NH-COOH-CP sample, the change in the crystal field stabilization energy from the ligand substitution showed an increase intensity and shift of the d-d band (maximum near 300 nm).[89]As shown in Fig. 4(a), the immobilization of a hydroxo-CP onto the carboxylate-modified LDHs was achieved through the coordination of π electron of carboxylate groups onto the d orbital of Platinum. The surface positive charge on LDH framework facilitates an increase in the particle cellular internalization via endocytosis because of their high affinity towards negatively charged cell membranes. When the LDH-NH-COOH-CP complexes were uptaken by the cancer cells, the acidic pH values of endosomal or lysosomal environments weaken the carboxylate coordination with Platinum. Furthermore, a high concentration of nucleophiles such as the cytosol Cl- ions and H2O molecules may replace the carboxylate groups to release the CP molecules into cytosol. The released CP molecules can efficiently diffuse into the nucleus and covalently bind with the DNA bases. This binding can result in the production of DNA cross-links, which may alter the DNA conformation and influence the transcriptional and translational process leading to an irreparable DNA damage resulting in apoptosis. It is evident from the release curve attained which represents that the sensitivity of the coordination is weaker in endosome pH (5.0) than the PBS (pH-7.4) (Fig. 4b). This follows the above proposed mechanistic release to act against cancer cells. Cellular internalization of Cy5.5 labelled LDH-NH-COOH-CP was ample higher and can be observed using the amount of red fluorescence emitted by NIR-contrast agent Cy5.5 because of charge neutralization after cisplatin conjugation (Fig. 5a).

It is clear from the image that LDH nanocontainers observed are very near to the nucleus and can be a supportive evidence for the delivery of cisplatin. Nucleus shrinkage was observed in the treated cells after stained with DAPI that quote the successful cisplatin delivery in the cell as shown in Fig. 5b and the shrunken nucleus was pointed out with arrows. Fig. S4 represents the cell morphology of HT-29 before (Fig. S4(a)) and after treatment with LDH-NH-COO-CP complexes for 24 h at concentrations of 10 (Fig. S4(b)), 50 (Fig. S4(c)) and 100 (Fig. S4(d)) μg mL^{-1}. Nanoparticles devoid of Hydroxo substituted cisplatin (LDH-NH-PEG5000, LDH-NH-COOH) weren't cytotoxic even at the higher concentrations (100 μg mL^{-1}) (Fig. S4(e, f)). If we compare the cell morphology between the untreated (Fig 5 b control) and treated samples (Fig. 5b treatment), shrinkage is noted in particle treated cells indicating massive apoptotic cell death of the cancer cells. When we compare the morphology of cells treated with different concentrations of drug loaded particles, cell shrinkage is observed in a dose dependent manner.

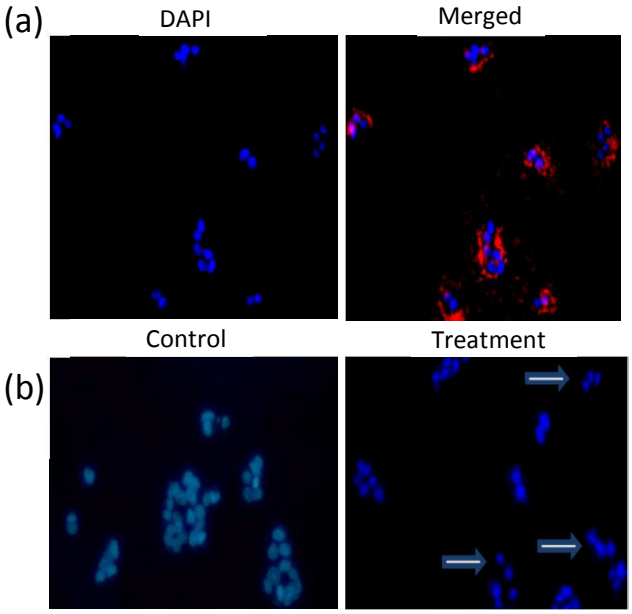

Fig. 5 Fluorescent microscopy of the cellular uptake behavior of Cy5.5-labeled LDH-NH-COOH-CP samples in HT-29 cancer cells (a) DAPI and merged image (LDH complexes denoted via red fluorescence of Cy5.5, and nuclei denoted via blue fluorescence of DAPI staining). (b) DAPI stain alone representing the shrunken nucleus in control and after treatment at 37 °C for 4 h.

To evaluate the cytotoxicity of LDH, LDH-NH_2, LDH-NH-PEG5000 and LDH-NH-COOH samples, we measured the cell viability using different LDH samples in the HT-29 colon cell line by MTT cytotoxicity assay (Fig. S5). The

HT-29 cells were treated with different LDH samples at various concentrations (0, 3, 5, 13, 25, 40, 50, and 80 μg mL^{-1}) diluted in media for 24 h. Cells without nanoparticles were taken as the control experiment, and the viability was set as 100%. The cell viability of the naked LDH samples gradually decreased from 100% (3 μg mL^{-1}) to 70% (80 μg mL^{-1}) treatment. A decrease in the cell viability with naked LDH nanoparticles may arise from the high nonspecific interactions between the naked LDH surfaces and the biological molecules. The naked LDH surfaces possess high activation energy which may cause the denaturation of protein or enzyme molecules. After surface functionalizing the LDH samples with different functional groups (LDH-NH_2, LDH-NH-PEG5000, and LDH-NH-COOH), it is observed that the particles did not induce any cytotoxicity even at very high concentration and for long-time exposure in HT-29 cells. The low cytotoxicity of functionalized LDH possibly results from the reduction of nonspecific interactions of the nanoparticle with the biological systems. Thus, it is always advantageous to functionalize LDH nanoparticles to increase the drug loading capability and biocompatibility by reducing the cytotoxicity. Additionally, the functionalized nanoparticles can provide high surface area to attach various charged functional groups that can regulate the biodistribution of drugs at the desired site. We also performed lactate dehydrogenase release assay to evaluate the cell membrane damage of the cells treated with surface functionalized particles (Fig. S6). Lactate dehydrogenase assay quantitatively measures the activity of the lactate dehydrogenase enzyme that is released up on the cell membrane damage. For this experiment, the maximal release of positive control was obtained by the treatment of control cells (no nanoparticle added) with 0.5% Triton X-100 for 10 min at room temperature. Compared with the control experiment (CTL), the LDH, LDH-NH2, LDH-NH-PEG 5000, and LDH-NH-COOH samples did not show a profound increase in the release of lactate dehydrogenase after treatment with various concentrations (0, 10, 50, and 100 μg mL-1) for 24 h. When we treated LDH-NH-COOH-CP complexes with the concentration of 50 and 100 μg mL-1, we observed that the release of lactate dehydrogenase was less than the CTL cells. We referred a decreasing release of lactate dehydrogenase from the anti-proliferative effect of the conjugated CP molecules. From the results obtained from the lactate dehydrogenase assay, it is concluded that both the functionalized and drug-conjugated LDH nanoparticles are highly biocompatible, retaining the membrane integrity by decreasing the unexpected necrotic cell death.

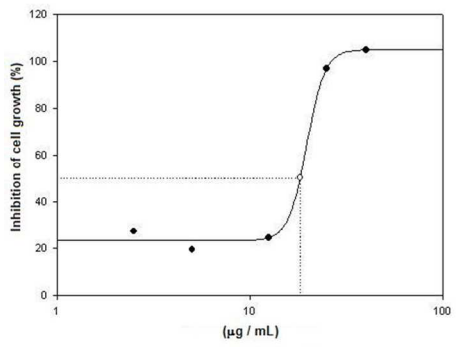

Fig. 6 GI_{50} from the SRB assay of LDH-NH-COOH-CP nanoparticles to colon cancer cells (HT-29). Various concentrations of LDH-NH-COOH-CP nanoparticles were added to cells for 24 h. Then, cells were fixed, stained with SRB, washed with dd-H_2O, subsequently solubilized and finally absorbance was read at a wavelength of 515 nm.

A majority of the anticancer drugs induce cell death either by apoptotic pathway or necrotic pathway. Induction of cell death by employing apoptotic path way confers many advantages over necrotic pathway as cell death induced by necrotic pathway involves the breakage of cell membrane releasing the cytokines that can trigger inflammatory responses, which in turn can result in poor prognosis. To further evaluate the anticancer effect of the LDH-NH-COOH-CP complexes, we used a sulforhodamine B assay to examine the inhibitive effects on cell proliferation by treating with free CP and LDH-NH-COOH-CP complexes. The data showed that LDH-NH-COOH-CP complexes efficiently inhibited the cell growth of HT-29 cells in a dose dependent manner with the 50% growth inhibition (GI50) at 18.1 μg mL^{-1} (Fig. 6).

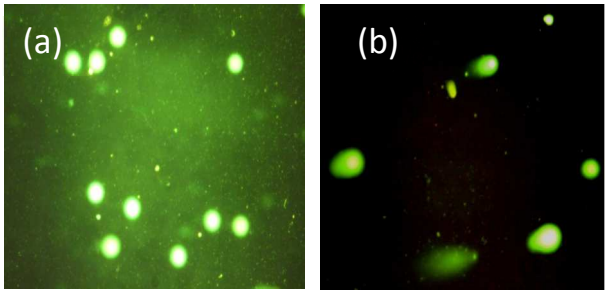

Fig. 7 Comet assay of HT-29 cells to detect DNA strand breaks. The cell apoptosis was produced by cisplatin to induce DNA damage and activate various signaling pathways. We used a fluorescent microscope (Olympus CKX41) fitted with 100W mercury illumination system suitable for fluorescence (SYBR Green) observations. Photographs of DNA strands after the treatment with 50 μg mL^{-1} of (a) LDH-NH-COOH and (b) LDH-NH-COOH-CP.

The loading percentages of CP molecules in LDH-NH-COOH-CP complexes is 10.8 (wt%) so we can calculate that the GI50 of the LDH-NH-COOH-CP complexes is 2.0 μg mL^{-1} of the free CP concentration. We also evaluated the anti-proliferative effect of free CP molecules in the same cancer cell line which showed a higher GI50 values (61.7 μg mL^{-1}). From these studies, we confirm that LDH-NH-COOH-CP complexes have higher proliferative index in cancer cell lines. This enhanced anti-proliferative effect appears to be primarily attributed to the efficient drug delivery of the LDH nanocarriers and the pH controlled release of carboxylate coordination of CP in the acidic endosomal environments. Furthermore, the release of CP can further escape endosomes. Additionally, a significant decrease in viability is noted in cells treated with drug loaded particles when compared to the controls which resulted from the high anti-proliferative effect induced by apoptosis. From the experimental data, it is observed that the cell membrane integrity remained unaltered which confirms that cell death is not induced by necrotic pathway. The lower levels of anti-proliferative effect of free CP molecules is due to the simple diffusion mechanism of free drug where as LDH loaded drug

entities have higher anti-proliferative effect due to the clathrin-dependent endocytosis. To further confirm apoptotic cell death, we performed DNA fragmentation assay (a signet of apoptosis). We measured the genotoxicity of LDH-NH-COOH-CP complexes by treating with different concentrations of particles (5 and 10.3 μg mL^{-1} for 24 h) (Fig. S7) DNA fragmentation assays were performed by electrophoresis on 2.0% agarose gels. After electrophoresis, gels were stained with ethidium bromide and examined under UV light and photographed with an image analysis system. The pattern of dose response showed an initial decrease in DNA damaging effect at lower concentration (5 μg mL^{-1}) followed by an increase at the highest concentration (10.3 μg mL^{-1}). DNA damaging potential of LDH-NH-COOH and LDH-NH-COOH-CP was also observed in HT-29 cells by performing comet assay (Fig. 7). The results showed significant genotoxicty in LDH-NH-COOH-CP complexes (Fig. 7b) when compared to LDH-NH-COOH treated cells (Fig. 7a). The mechanism of action by which LDH-NH-COOH-CP complexes causes DNA damage is not fully understood from our results. One of the possible mechanisms is via the binding of drug with the DNA and thereby halting the processes such as replication and transcription leading to apoptosis.

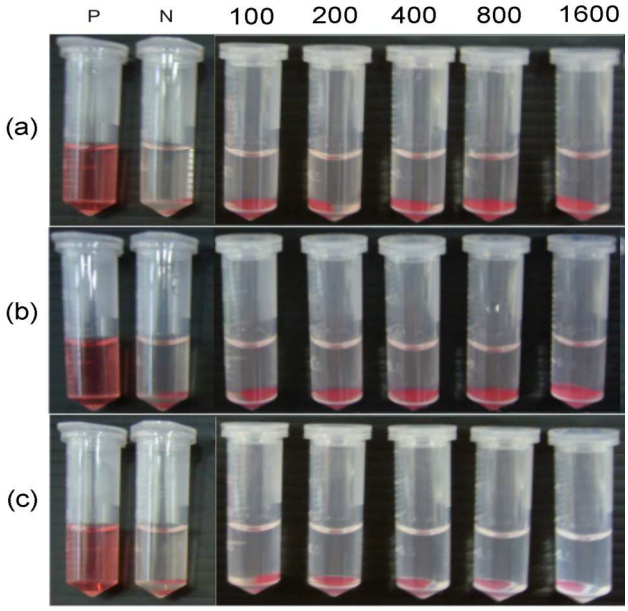

Fig. 8 Photographs of hemolysis of RBCs after the treatment of 100, 200, 400, 800, 1600 μg mL^{-1} of (a) LDH-NH_2, (b) LDH-NH-PEG5000, and (c) LDH-NH-COOH samples for 3 h. The red hemoglobin in the supernatant indicated the damage of RBCs in the positive control experiment. dd-H_2O and PBS are used as positive (P) and negative (N) controls, respectively.

To further evaluate the *in vivo* toxicity of the LDH-NH-COOH-CP complexes, we performed a hemolytic assay. This assay measures the release of hemoglobin from the cells resulting from red blood cell destruction and estimates the extent of RBC hemolysis. For hemolytic assay, we incubated various particles with different concentrations (100, 200, 400, 800, and 1600 μg mL^{-1}) with RBCs for 3 h and the results were as shown in Fig. 8. The exposure of LDH-NH_2, LDH-NH-PEG5000, and LDH-NH-COOH samples to RBCs did not induce hemolysis; therefore, we can confirm that the surface functionalized LDH nanoparticles are highly biocompatible and non-toxic, even at very high concentrations. To increase the therapeutic efficacy and reduce the deleterious side effects there is a need to design site-specific delivery systems which can significantly reduce the drug dosage thereby reducing the toxicity resulting from the drug accumulation in the off targeted sites. To meet this challenge, we regulated the surface properties on LDH nanoparticles that efficiently delivered the drug in the targeted organ. We studied the biodistribution of LDH-NH_2, LDH-NH-PEG5000, and LDH-NH-COOH samples in the animal model by using a NIR fluorescent dye (Cy 5.5) as an optical contrast agent. To get a solid prove for the distribution of the functionalized LDH nanoparticles, we traced the fluorescent stability of various modification of LDH-Cy5.5 samples in blood plasma for 3 h. The results showed the fluorescent intensity is stable in plasma and there is no leaching of fluorescent dye (Cy5.5) from LDH surfaces because the centrifuged pellets have very high fluorescent intensity and the supernatant of blood plasma is clear and not fluorescent. Thus, the combination of functionalized LDHs and Cy 5.5 can provide the high stability and efficiency for *in vivo* optical imaging because the excitation and emission at long wavelengths (ex: 678 nm; em: 703 nm) in the NIR window minimizes the intrinsic background interference since blood and tissue are relatively transparent in this range.

(a)

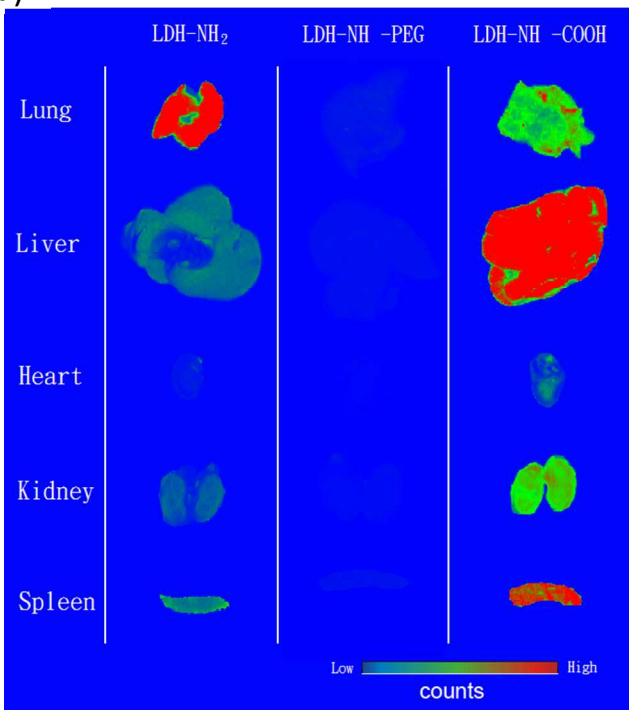

(b)

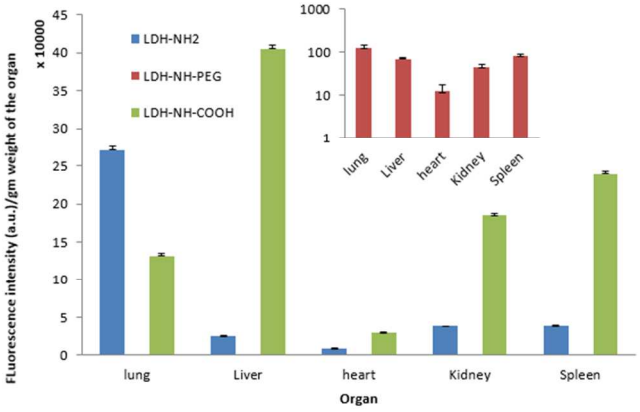

Fig. 9 (a) Fluorescent images of dissected organs from a mouse sacrificed after i.v. injection of Cy5.5-labeled LDH-NH_2, LDH-NH-PEG 5000 and LDH-NH-COOH for 3 h. (b) graphical representation of quantitative distribution of fluorescence with respective each organ.

In order to confirm the fluorescent intensity in each organs, a typical ex vivo organ optical imaging of sacrificed mice after an i.v. injection of various LDH samples for 3 h is acquired and showed in Fig. 9a. To compare the relative fluorescent intensity of various samples, the organs were imaged using the same intensity of PMT at 250V and Fig. 9a was represented in the same scale range. We observed that the relative intensity of fluorescence of the LDH-NH_2 samples remained mainly in the lungs. Lung accumulation of positive LDH-NH_2 may arise due to the non-specific electrostatic interaction between the positive charges of LDH-NH_2 surfaces and the negative charges of cellular membranes. Indeed, the first organs for nanoparticle influx by i.v. injection were the lungs, and the capillary circulation usually causes a slower blood flow in the lungs; therefore, the LDH-NH_2 nanoparticles maybe rapidly uptaken by lung epithelial and macrophage cells. To prolong the circulation time and decrease the rapid clearance from the biological systems, we modified the LDH-NH_2 surfaces with PEG5000 molecules. We can observe a comparatively less accumulation of LDH-NH-PEG 5000 samples, in all the five organs (Fig. 9b). It has been reported that PEG modification provides a steric shield around the particle shells, effectively preventing plasma proteins from adsorption to the particle surface and thus avoiding subsequent uptake by macrophages in the reticuloendothelial system. In case of negatively charged carboxylate-LDHs, nanoparticle accumulation in the lung was relative lower than the positive charged amino-LDHs. However, there is a significant accumulation of carboxylate-modified LDHs in the liver (Fig. 9b). We can speculate the difference in the biodistribution of the opposite charged LDHs to the decrease of affinity of negatively charged carboxylate-LDHs with lung macrophage cells, and epithelial cells; therefore, carboxylate-modified LDHs can retain in the blood circulation and pass the lung. The large accumulation of LDH-NH-COOH samples in liver may arise from the uptake contribution from the liver hepatocellular cells. Partial accumulation of nanoparticles in spleen may arise from the cleared effect from the uptake by the reticuloendothelial system and the mononuclear phagocytic system which were largely present in the spleen and bone marrow.

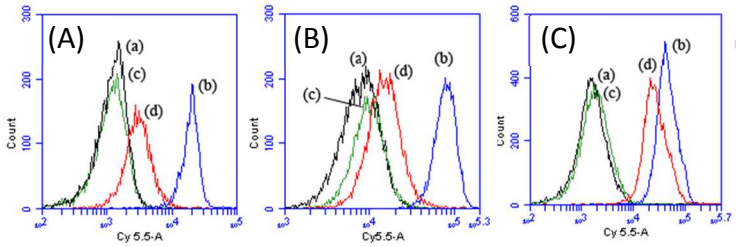

Fig. 10 Flow cytometric analyses of cellular uptake of LDH samples in (A) Raw 264.7, (B) A549, and (C) Hep G2 cells for 1 h. (a) control cells without nanoparticle treatment (black line), (b) LDH-NH_2 (blue line), (c) LDH-NH-PEG 5000 (green line), and (d) LDH-NH-COOH (red line) samples.

To explain the comparative *in vivo* biodistribution profile of the three types of nanoparticles, an *in vitro* experiment of flow cytometry to evaluate their uptake by RAW264.7 (mouse macrophage cell), A549 (human lung epithelial cell), and Hep G2 (liver hepatocellular) cell lines was carried out (Fig. 10).

It is evident from the flow cytometry results that the positively charged LDH-NH_2 nanoparticles have the highest level of cellular uptake in all the three cell lines. Thus, the particles administered through i.v. tail vein injection, first circulated in the lungs and thereby resulting in significant particle accumulation in the lungs by non-specific uptake of lung epithelial and macrophage cells. The PEG5000-modified LDH samples displayed a decreased level of non-specific cellular uptake in all the three cell lines which is evident from the low cellular fluorescent intensity level that is similar to control groups (untreated cell lines). The modification of PEG5000 polymer is believed to provide a steric shield around the particle surfaces thereby prolonging the particle circulation in the blood through decreased uptake by lungs, liver and the resident phagocytes. In case of LDH-NH-COOH samples, the cellular uptake results showed that the negatively charged nanoparticle surfaces have much less affinity towards RAW264.7 and A549 cell lines. However, a significant uptake is seen in Hep G2 cell lines demonstrating their ability to interact with liver. The in vitro cellular uptake experiments from flow cytometry are relevant to effects observed in vivo.

Conclusions

In summary, our findings suggest that charge functionalized LDH nanoparticles have an enormous potential to serve as tools for noninvasive imaging and organ specific drug delivery. An increased number of carboxyl groups in the layered structure enhanced the drug-loading capacity and the stability of poor water soluble drug Cisplastin thus minimizing the off-target toxicity. The excellent biocompatibility of functionalized LDH was demonstrated by its negligible red blood cell hemolysis and lactate dehydrogenase release even at extremely high concentrations. We have shown that drug conjugated

nanoparticle (LDH-NH-COOH-CP) complexes have a high anti-proliferative effect on the colon cancer cell lines when compared with the administration of free drug demonstrating the efficacy of LDH nanoparticles as drug carriers. Interestingly, the un-charged LDH-NH-PEG5000 particles have a very low macrophageal uptake in the reticuloendothelial system (RES) thereby increasing the blood circulation with low levels of particle accumulation in the major organs. Additionally, the encapsulation of the drug molecule in the layered structure facilitated safe transportation of the drug molecules to the targeted site avoiding the drug leakage in the off-targeted sites. The use of LDH nanoparticles as drug delivery vehicles bear many advantages over other nano carriers as they bear a net positive charge on their surface which can aid the binding of various functional groups, biological moieties and imaging agents bearing negative charges to achieve organ-specific drug delivery along with simultaneous diagnosis.

Acknowledgements

We are very thankful to the Ministry of Science and Technology, Taiwan for research grants (NSC 101-2113-M-259-003-MY2, MOST 103-2113-M-259-005-MY2).

Notes and references

1. J. H. Lee and D. Y. Jung, *Chem. Commun.*, 2012, 48, 5641-5643.
2. M. Chakraborti, J. K. Jackson, D. Plackett, S. E. Gilchrist and H. M. Burt, *J. Mater. Sci.-Mater. Med.*, 2012, 23, 1705-1713.
3. K. Minagawa, M. R. Berber, I. H. Hafez, T. Mori and M. Tanaka, *J. Mater. Sci.-Mater. Med.*, 2012, 23, 973-981.
4. S. J. Xia, Z. M. Ni, Q. Xu, B. X. Hu and J. Hu, *J. Solid State Chem.*, 2008, 181, 2610-2619.
5. L. Tammaro, U. Costantino, M. Nocchetti and V. Vittoria, *Appl. Clay Sci.*, 2009, 43, 350-356.
6. B. X. Li, J. He, D. G. Evans and X. Duan, *Int. J. Pharm.*, 2004, 287, 89-95.
7. F. S. Li, L. Jin, J. B. Han, M. Wei and C. J. Li, *Ind. Eng. Chem. Res.*, 2009, 48, 5590-5597.
8. X. G. Kong, S. X. Shi, J. B. Han, F. J. Zhu, M. Wei and X. Duan, *Chem. Eng. J.*, 2010, 157, 598-604.
9. X. G. Kong, L. Jin, M. Wei and X. Duan, *Appl. Clay Sci.*, 2010, 49, 324-329.
10. R. F. P. I. F. ALEXA, M. IGNAT, E. POPOVICI* and V. A. V. *Corresponding author: , *Digest Journal of Nanomaterials and Biostructures*, 2011, 6, 1091-1101.
11. S. H. Hussein Al Ali, M. Al-Qubaisi, M. Z. Hussein, M. Ismail, Z. Zainal and M. N. Hakim, *Int J Nanomedicine*, 2012, 7, 2129-2141.
12. H. Zhang, D. K. Pan and X. Duan, *J. Phys. Chem. C*, 2009, 113, 12140-12148.
13. Z. Xu, Z. Gu, X. Cheng, F. Rasoul, A. Whittaker and G. Lu, *Journal of Nanoparticle Research*, 2011, 13, 1253-1264.
14. S.-J. Choi, G. E. Choi, J.-M. Oh, Y.-J. Oh, M.-C. Park and J.-H. Choy, *Journal of Materials Chemistry*, 2010, 20, 9463-9469.
15. H. Zhang, D. K. Pan, K. Zou, J. He and X. Duan, *J. Mater. Chem.*, 2009, 19, 3069-3077.
16. S. J. Choi, J. M. Oh and J. H. Choy, *J. Nanosci. Nanotechnol.*, 2008, 8, 5297-5301.
17. S. J. Choi, J. M. Oh and J. H. Choy, *J. Inorg. Biochem.*, 2009, 103, 463-471.
18. S. J. Choi, J. M. Oh and J. H. Choy, *J Nanosci Nanotechnol*, 2010, 10, 2913-2916.
19. J. M. Oh, D. H. Park, S. J. Choi and J. H. Choy, *Recent Pat Nanotechnol*, 2012.
20. D. Li, X. Xu, J. Xu and W. Hou, *Colloids and Surfaces A: Physicochemical and Engineering Aspects*, 2011, 384, 585-591.
21. M. Baek, I. S. Kim, J. Yu, H. E. Chung, J. H. Choy and S. J. Choi, *J. Nanosci. Nanotechnol.*, 2011, 11, 1803-1806.
22. H. Hu, K. M. Xiu, S. L. Xu, W. T. Yang and F. J. Xu, *Bioconjugate chemistry*, 2013, 24, 968-978.
23. Z. P. Xu, T. L. Walker, K. L. Liu, H. M. Cooper, G. Q. M. Lu and P. F. Bartlett, *Int. J. Nanomed.*, 2007, 2, 163-174.

24. K. Ladewig, Z. P. Xu and G. Q. Lu, *Expert Opin. Drug Deliv.*, 2009, 6, 907-922.
25. K. Ladewig, M. Niebert, Z. P. Xu, P. P. Gray and G. Q. Lu, *Appl. Clay Sci.*, 2010, 48, 280-289.
26. Z. P. Xu, T. L. Walker, K. L. Liu, H. M. Cooper, G. Q. Lu and P. F. Bartlett, *Int J Nanomedicine*, 2007, 2, 163-174.
27. Y. Wong, K. Markham, Z. P. Xu, M. Chen, G. Q. Max Lu, P. F. Bartlett and H. M. Cooper, *Biomaterials*, 2010, 31, 8770-8779.
28. Y. Y. Wong, H. M. Cooper, K. Zhang, M. Chen, P. Bartlett and Z. P. Xu, *J. Colloid Interface Sci.*, 2012, 369, 453-459.
29. M. Chen, H. M. Cooper, J. Z. Zhou, P. F. Bartlett and Z. P. Xu, *Journal of colloid and interface science*, 2013, 390, 275-281.
30. Z. Gu, B. E. Rolfe, Z. P. Xu, J. H. Campbell, G. Q. Lu and A. C. Thomas, *Advanced Healthcare Materials*, 2012, DOI: 10.1002/adhm.201200069, n/a-n/a.
31. Z. Gu, B. E. Rolfe, A. C. Thomas, J. H. Campbell, G. Q. Lu and Z. P. Xu, *Biomaterials*, 2011, 32, 7234-7240.
32. Y. Wang, Z. Wang, Y. Rui and M. Li, *Biosensors & bioelectronics*, 2015, 64, 57-62.
33. B. Saifullah, M. E. El Zowalaty, P. Arulselvan, S. Fakurazi, T. J. Webster, B. M. Geilich and M. Z. Hussein, *Drug design, development and therapy*, 2014, 8, 1029-1036.
34. B. Saifullah, P. Arulselvan, M. E. El Zowalaty, S. Fakurazi, T. J. Webster, B. M. Geilich and M. Z. Hussein, *International journal of nanomedicine*, 2014, 9, 4749-4762.
35. Z. Gu, A. Wu, L. Li and Z. P. Xu, *Pharmaceutics*, 2014, 6, 235-248.
36. Z. Gu, J. J. Atherton and Z. P. Xu, *Chem Commun (Camb)*, 2015, DOI: 10.1039/c4cc07715f.
37. M. Badar, M. I. Rahim, M. Kieke, T. Ebel, M. Rohde, H. Hauser, P. Behrens and P. P. Mueller, *Journal of biomedical materials research. Part A*, 2014, DOI: 10.1002/jbm.a.35358.
38. S. Yan, B. E. Rolfe, B. Zhang, Y. H. Mohammed, W. Gu and Z. P. Xu, *Biomaterials*, 2014, 35, 9508-9516.
39. M. Halma, C. Mousty, C. Forano, M. Sancelme, P. Besse-Hoggan and V. Prevot, *Colloids and Surfaces B: Biointerfaces*, DOI: http://dx.doi.org/10.1016/j.colsurfb.2014.11.029.
40. L. Qin, W. Wang, S. You, J. Dong, Y. Zhou and J. Wang, *International journal of nanomedicine*, 2014, 9, 5701-5710.
41. K. Ladewig, M. Niebert, Z. P. Xu, P. P. Gray and G. Q. M. Lu, *Biomaterials*, 2010, 31, 1821-1829.
42. V. R. R. Cunha, A. M. D. Ferreira, V. R. L. Constantino, J. Tronto and J. B. Valim, *Quim. Nova*, 2010, 33, 159-171.
43. T.-H. Kim, H. J. Kim and J.-M. Oh, *Journal of Nanomaterials*, 2012, 2012, 7.
44. Z. Gu, B. E. Rolfe, Z. P. Xu, A. C. Thomas, J. H. Campbell and G. Q. M. Lu, *Biomaterials*, 2010, 31, 5455-5462.
45. Z. P. Xu, M. Niebert, K. Porazik, T. L. Walker, H. M. Cooper, A. P. J. Middelberg, P. P. Gray, P. F. Bartlett and G. Q. Lu, *J. Control. Release*, 2008, 130, 86-94.
46. S. Sun and W. G. Hou, *Chinese Chemical Letters*, 2007, 18, 1371-1373.
47. D. Yan, J. Lu, M. Wei, D. G. Evans and X. Duan, *J Phys Chem B*, 2009, 113, 1381-1388.
48. J. M. Oh, C. B. Park and J. H. Choy, *J. Nanosci. Nanotechnol.*, 2011, 11, 1632-1635.
49. S. J. Choi, G. E. Choi, J. M. Oh, Y. J. Oh, M. C. Park and J. H. Choy, *J. Mater. Chem.*, 2010, 20, 9463-9469.
50. L. Yan, W. Chen, X. Zhu, L. Huang, Z. Wang, G. Zhu, V. A. Roy, K. N. Yu and X. Chen, *Chemical communications*, 2013, 49, 10938-10940.

51. M. Yan, Z. Zhang, S. Cui, M. Lei, K. Zeng, Y. Liao, W. Chu, Y. Deng and C. Zhao, *International journal of nanomedicine*, 2014, 9, 4867-4878.
52. S. J. Choi, J. M. Oh and J. H. Choy, *J. Nanosci. Nanotechnol.*, 2010, 10, 2913-2916.
53. L. Li, W. Gu, J. Chen, W. Chen and Z. P. Xu, *Biomaterials*, 2014, 35, 3331-3339.
54. T. H. Kim, G. J. Lee, J. H. Kang and H. J. Kim, 2014, 2014, 193401.
55. A. N. Ay, B. Zumreoglu-Karan, A. Temel and V. Rives, *Inorg Chem*, 2009, 48, 8871-8877.
56. J. Chen, R. Shao, L. Li, Z. P. Xu and W. Gu, *International journal of nanomedicine*, 2014, 9, 3403-3411.
57. C. Chen, L. K. Yee, H. Gong, Y. Zhang and R. Xu, *Nanoscale*, 2013, 5, 4314-4320.
58. L. Wang, H. Xing, S. Zhang, Q. Ren, L. Pan, K. Zhang, W. Bu, X. Zheng, L. Zhou, W. Peng, Y. Hua and J. Shi, *Biomaterials*, 2013, 34, 3390-3401.
59. D. Li, Y. T. Zhang, M. Yu, J. Guo, D. Chaudhary and C. C. Wang, *Biomaterials*, 2013, 34, 7913-7922.
60. G. Stoica, I. Castello Serrano, A. Figuerola, I. Ugarte, R. Pacios and E. Palomares, *Nanoscale*, 2012, 4, 5409-5419.
61. S. N. Ding, D. Shan, T. Zhang and Y. Z. Dou, *Journal of Electroanalytical Chemistry*, 2011, 659, 1-5.
62. S. Bégu, A. Aubert-Pouëssel, R. Polexe, E. Leitmanova, D. A. Lerner, J.-M. Devoisselle and D. Tichit, *Chemistry of Materials*, 2009, 21, 2679-2687.
63. J. Huang, G. Gou, B. Xue, Q. Yan, Y. Sun and L. E. Dong, *Int J Pharm*, 2013, 450, 323-330.
64. X. Bi, T. Fan and H. Zhang, *ACS applied materials & interfaces*, 2014, 6, 20498-20509.
65. L. N. M. Ribeiro, A. C. S. Alcântara, M. Darder, P. Aranda, P. S. P. Herrmann Jr, F. M. Araújo-Moreira, M. García-Hernández and E. Ruiz-Hitzky, *International journal of pharmaceutics*, 2014, 477, 553-563.
66. A. C. S. Alcantara, P. Aranda, M. Darder and E. Ruiz-Hitzky, *J. Mater. Chem.*, 2010, 20, 9495-9504.
67. M. Z. Hussein, N. F. B. Nazarudin, S. H. Sarijo and M. A. Yarmo, *Journal of Nanomaterials*, 2012, DOI: 860352 10.1155/2012/860352.
68. J. Liu, R. Harrison, J. Z. Zhou, T. T. Liu, C. Yu, G. Q. Lu, S. Z. Qiao and Z. P. Xu, *Journal of Materials Chemistry*, 2011, 21, 10641-10644.
69. D. Pan, H. Zhang, T. Fan, J. Chen and X. Duan, *Chemical Communications*, 2011, 47, 908-910.
70. Y.-E. Miao, H. Zhu, D. Chen, R. Wang, W. W. Tjiu and T. Liu, *Materials Chemistry and Physics*, 2012, 134, 623-630.
71. G. Kapusetti, N. Misra, V. Singh, R. K. Kushwaha and P. Maiti, *Journal of Biomedical Materials Research Part A*, 2012, 100A, 3363-3373.
72. H. Hu, X. B. Wang, S. L. Xu, W. T. Yang, F. J. Xu, J. Shen and C. Mao, *J. Mater. Chem.*, 2012, 22, 15362-15369.
73. H. Bao, J. Yang, Y. Huang, Z. P. Xu, N. Hao, Z. Wu, G. Q. Lu and D. Zhao, *Nanoscale*, 2011, 3, 4069-4073.
74. P.-R. Wei, S.-H. Cheng, W.-N. Liao, K.-C. Kao, C.-F. Weng and C.-H. Lee, *Journal of Materials Chemistry*, 2012, 22, 5503-5513.
75. L. Yan, Y. Wang, J. Li, S. Kalytchuk, A. S. Susha, S. V. Kershaw, F. Yan, A. L. Rogach and X. Chen, *Journal of Materials Chemistry C*, 2014, 2, 4490-4494.
76. W. Shi, Y. Fu, Z. Li and M. Wei, *Chemical Communications*, 2015, 51, 711-713.
77. D. Li, L. Qian, Y. Feng, J. Feng, P. Tang and L. Yang, *ACS applied materials & interfaces*, 2014, 6, 20603-20611.

78. X. Q. Zhang, M. G. Zeng, S. P. Li and X. D. Li, *Colloids and surfaces. B, Biointerfaces*, 2014, 117, 98-106.
79. G. Layrac, M. Destarac, C. Gerardin and D. Tichit, *Langmuir*, 2014, 30, 9663-9671.
80. D. Y. Tian, Z. L. Liu, S. P. Li and X. D. Li, *Materials science & engineering. C, Materials for biological applications*, 2014, 45, 297-305.
81. M. A. Dobrovolskaia, P. Aggarwal, J. B. Hall and S. E. McNeil, *Molecular pharmaceutics*, 2008, 5, 487-495.
82. R. Ma, Z. Wang, L. Yan, X. Chen and G. Zhu, *Journal of Materials Chemistry B*, 2014, 2, 4868-4875.
83. D. W. Knapp, R. C. Richardson, P. L. Bonney and K. Hahn, *J Vet Intern Med*, 1988, 2, 41-46.
84. G. Cavaletti, M. G. Petruccioli, G. Tredici, P. Marmiroli, I. Barajon, D. Fabbrica and A. Di Francesco, *Int J Tissue React*, 1991, 13, 151-157.
85. J.-M. Oh, S.-J. Choi, G.-E. Lee, S.-H. Han and J.-H. Choy, *Advanced Functional Materials*, 2009, 19, 1617-1624.
86. Z. P. Xu, G. S. Stevenson, C. Q. Lu, G. Q. Lu, P. F. Bartlett and P. P. Gray, *J Am Chem Soc*, 2006, 128, 36-37.
87. K. Ladewig, M. Niebert, Z. P. Xu, P. P. Gray and G. Q. Lu, *Biomaterials*, 2010, 31, 1821-1829.
88. Z. P. Xu, G. Stevenson, C. Q. Lu and G. Q. Lu, *J Phys Chem B*, 2006, 110, 16923-16929.
89. N. Nishiyama, M. Yokoyama, T. Aoyagi, T. Okano, Y. Sakurai and K. Kataoka, *Langmuir*, 1998, 15, 377-383.